Journal of Pharmaceutical Analysis 14 (2024) 100974

Contents lists available at ScienceDirect

Journal of Pharmaceutical Analysis

journal homepage: www.elsevier.com/locate/jpa

Original article

Structural characterization and mechanisms of macrophage immunomodulatory activity of a novel polysaccharide with a galactose backbone from the processed Polygonati Rhizoma

Hongna Su [a], Lili He [a], Xina Yu [a], Yue Wang [b], Li Yang [b], Xiaorui Wang [a], Xiaojun Yao [c], Pei Luo [a, *], Zhifeng Zhang [a, b, **]

[a] Faculty of Chinese Medicine, State Key Laboratory of Quality Research in Chinese Medicine, Macau University of Science and Technology, Macau, 999078, China
[b] Tibetan Plateau Ethnic Medicinal Resources Protection and Utilization Key Laboratory of National Ethnic Affairs Commission of the People's Republic of China, Southwest Minzu University, Chengdu, 610041, China
[c] Centre for Artificial Intelligence Driven Drug Discovery, Faculty of Applied Sciences, Macao Polytechnic University, Macau, 999078, China

ARTICLE INFO

Article history:
Received 21 September 2023
Received in revised form
5 February 2024
Accepted 28 March 2024
Available online 29 March 2024

Keywords:
Polygonati Rhizoma
Polysaccharide
Structural properties
Immunoregulatory

ABSTRACT

A purified polysaccharide with a galactose backbone (SPR-1, Mw 3,622 Da) was isolated from processed Polygonati Rhizoma with black beans (PRWB) and characterized its chemical properties. The backbone of SPR-1 consisted of [(4)-β-D-Gal*p*-(1]$_9$ → 4,6)-β-D-Gal*p*-(1 → 4)-α-D-Gal*p*A-(1 → 4)-α-D-Gal*p*A-(1 → 4)-α-D-Glc*p*-(1 → 4,6)-α-D-Glc*p*-(1 → 4)-α/β-D-Glc*p*, with a branch chain of R_1: β-D-Gal*p*-(1 → 3)-β-D-Gal*p*-(1→ connected to the →4,6)-β-D-Gal*p*-(1→ via O-6, and a branch chain of R_2: α-D-Glc*p*-(1 → 6)-α-D-Glc*p*-(1→ connected to the →4,6)-α-D-Glc*p*-(1→ via O-6. Immunomodulatory assays showed that the SPR-1 significantly activated macrophages, and increased secretion of NO and cytokines (i.e., IL-1β and TNF-α), as well as promoted the phagocytic activities of cells. Furthermore, isothermal titration calorimetry (ITC) analysis and molecular docking results indicated high-affinity binding between SPR-1 and MD2 with the equilibrium dissociation constant (K_D) of 18.8 μM. It was suggested that SPR-1 activated the immune response through Toll-like receptor 4 (TLR4) signaling and downstream responses. Our research demonstrated that the SPR-1 has a promising candidate from PRWB for the TLR4 agonist to induce immune response, and also provided an easily accessible way that can be used for PR deep processing.

1. Introduction

Polygonatum Rhizoma (PR), a functional edible herb, has been used to prevent and treat various diseases in traditional Chinese medicine (TCM) for a long history, such as the treatment of temporary or permanent immunity dysfunction, diabetes, spleen deficiency, coughs, anorexia, and stomach diseases [1,2]. At the same time, PR is also processed into a range of functional health products, such as PR wine, functional beverages, yogurt thickeners, and fermented foods [3,4]. Previous studies have reported that polysaccharides [2,5,6], flavonoids [7], and steroidal saponins [8] were the main chemical constituents of PR. Among these, polysaccharides have emerged as the primary biologically active components and have been officially recognized by the Chinese Pharmacopoeia as the key phytochemical marker for quality control, with a minimum required content of 7% [9].

The processing of raw herbs is an integral and distinctive pharmaceutical technique within TCM, playing a crucial role in mitigating side effects, enhancing medicinal properties, modifying characteristics, and even altering the therapeutic effects of these herbs [10]. Before its utilization in food and clinical applications, PR undergoes a necessary processing step to ensure its safety and efficacy [11]. Typically, PR is subjected to steaming, employing ingredients such as wine, black soybean, ginger, and honey [12–14]. Numerous studies have extensively reported notable changes in the chemical composition of PR following processing, and these

* Corresponding author.
** Corresponding author. Faculty of Chinese Medicine, State Key Laboratory for Quality Research in Chinese Medicines, Macau University of Science and Technology, Macau, 999078, China.
E-mail addresses: pluo@must.edu.mo (P. Luo), zfzhang@must.edu.mo (Z. Zhang).

https://doi.org/10.1016/j.jpha.2024.100974

alterations have the potential to significantly impact its biological activities [15]. Steaming with a black bean (BB) decoction is a special pre-treatment method commonly employed for some Chinese herbs before the drying process. This technique can be particularly beneficial for herbs containing toxic or irritating components. It is known to improve the liver and kidney nourishing effects while reducing the toxicity and side effects associated with these herbs [12]. An illustrative example is the study that revealed that emodin-8-*O*-β-D-glucoside, the primary anthraquinone component implicated in liver damage, exhibited lower content in the processed (BB) *Polygoni multiflori* Radix compared to the raw *P. multiflori* [16]. Moreover, the practice of washing or steaming Chinese medicines (CM) with beans is recognized as a distinctive technique for herbal fermentation within a composite matrix. This process can lead to alterations in certain chemical components and facilitate the release of active ingredients [17]. Processed PR with BB (PRWB) is a classic technique documented in Lu Mansion's Secrete Recipe classic which is a classic Chinese medical book of the Ming Dynasty. Previous studies mainly focused on water-steaming and wine-processing of PR. These studies have consistently reported that polysaccharides from PR mainly consisted of fructose, glucose, and galactose [2,6,9,11,18]. Fewer studies have reported the chemical components in PRWB, especially the polysaccharides with biologically active.

Polysaccharides are a class of macromolecular substances that are found in a wide range of species, including microorganisms, algae, plants, and animals [19]. Recently, polysaccharides have gained a lot of interest owing to their complex structure and a variety of biological activities, including antitumor [19–21], immunomodulatory [22,23], anti-inflammatory [24,25], hepatoprotective [26,27] and so on. A number of studies have shown that natural polysaccharides have remarkable anti-tumor activity without significant toxic and side effects [19]. Currently, polysaccharides have great potential to regulate cell signaling due to their structural multiplicity. Some polysaccharides can modulate the host immune system and indirectly play an anti-tumor role by pathways including activating non-specific or specific immune responses [28]. In fact, the effects of the Polygonatum polysaccharide (PP) on immune function have received a vast amount of attention due to their impact on human health and disease treatment. Previous studies have shown that the polysaccharides from PR exhibited potent immunomodulating properties, and could reverse immunosuppression by promoting immune organ development, lymphocyte proliferation, and macrophage phagocytosis as well as by regulating the levels of serum cytokines in immunosuppressive mice induced by cyclophosphamide (Cy) [29,30]. In recent years, some studies have found that the immunomodulatory activity of the PP was enhanced after concoction [3,7,31]. Nevertheless, the detailed chemical structures or mechanisms of immunomodulatory activity exhibited by the polysaccharides from PRWB have still not been reported.

Hence, it is essential to improve recognition of the composition, structural features, and bioactivity of the polysaccharides from PRWB and to probe the potential mechanism underlying the therapeutic immunomodulatory activity of the polysaccharides from PRWB to facilitate their further development and utilization as a safe and effective naturally produced drug as a novel immunomodulator. In this study, the polysaccharide was isolated and purified from PRWB and analyzed its structural features by high-performance gel permeation chromatography (HPGPC), Fourier-transform infrared (FT-IR), and nuclear magnetic resonance (NMR). Meanwhile, the polysaccharide was hydrolyzed and derivatized by acid to the partially methylated alditol acetates (PMAAs), which could be detected by gas chromatography-mass spectrometry (GC-MS). Furthermore, the immunomodulatory effects of the isolated polysaccharides on macrophages were observed and their potential mechanisms were further explored using isothermal titration calorimetry (ITC) and molecular docking.

2. Materials and methods

2.1. Materials and reagents

The PR was collected from Renshou County (Meishan, China) and identified by Professor Zhifeng Zhang (Macau University of Science and Technology, China). Dextrans of different molecular weights were purchased from Sigma-Aldrich Co., Ltd. (St. Louis, MO, USA). The monosaccharides including D-mannose (Man), L-rhamnose (Rha), D-galacturonic acid (GalA), D-galactose (Gal), D-glucose (Glc), D-glucuronic acid (GlcA), D-arabinose (Ara), D-xylose (Xyl), L-fucose (Fuc), D-glucosamine hydrochloride (GlcN), *N*-acetyl-D-glucosamine (GlcNA), D-fructose (Fru), D-ribose (Rib), D-galactosamine hydrochloride (GalN), L-guluronic acid (GulA) and D-mannuronic acid (ManA) were from BoRui Saccharide Biotech Co., Ltd (Yangzhou, China). Acetic anhydride, trifluoroacetic acid (TFA) and pyridine were all analytical grades and were purchased from Kermel Chemical Reagent Co., Ltd. (Tianjin, China). The dialysis bag (molecular of 3500 Da), tumour necrosis factor alpha (TNF-α) and interleukin-1beta (IL-1β) cytokine specific enzyme-linked immunosorbent assay (ELISA) kits and DEAE-52 were obtained from Solarbio Science &Technology Co., Ltd. (Beijing, China), and Milli-Q water was acquired through a Millipore system (Bedford, MA, USA). Lipopolysaccharide (LPS) was purchased from the Beyotime Institute of Biotechnology (Shanghai, China). MD2 protein was purchased from Sino Biological Inc. (Beijing, China). All the other chemicals and reagents were of analytical grade.

2.2. Preparation of PRWB and extraction of the polysaccharides

The most common method to extract polysaccharides from plants is hot water extraction [32]. The detailed flow chart for the extraction, isolation, and purification of the polysaccharide from PRWB was shown in Fig. S1. In brief, 8.5 kg of defatted and dried PRWB were pre-soaked in water for 1 h at room temperature, and extracted with 25 L of boiling distilled water for 3 h. In total, three extractions were performed. After that, the extracts were combined and concentrated to one-tenth volume, and ethanol was added in concentrate to a final concentration of 40% (*V/V*) and placed to precipitate for 24 h at 4 °C. The precipitate was obtained by centrifugation for 10 min (15,000 *g*) and the supernatant was removed. The obtained precipitates were freeze-dried and re-solubilized with water, and proteins were completely eliminated at least four times through the Sevag method to obtain the crude polysaccharide I (CP-I) [25]. The CP-I was then dissolved in distilled water to obtain 0.5 g/mL of the solution. The CP-I was gradually eluted through a DEAE-52 cellulose column (Φ3.5 cm × 80 cm) with distilled water, 0.05, 0.1, 0.2, 0.3, 0.4, 0.5 and 1.0 mol/L NaCl. Next, 10 mL of each tube was collected and determined using the phenol-sulfuric acid method to plot the elution curve [33]. The elution curve (Fig. 1A) showed that the one main peak only of the elution curve obtained by pure water elution was higher, so the pure water fraction was selected for further separation. The relevant eluents were concentrated and dialyzed using a 3,500 Da dialysis bag, and one relatively pure polysaccharide was obtained, referred to as SPR-1.

2.3. Characterization of SPR-1

2.3.1. Homogeneity and molecular weight analysis of SPR-1

The Mw and homogeneity of SPR-1 were measured using HPGPC based on a Shimadzu LC-10A system (Shimadzu, Kyoto, Japan) fitted

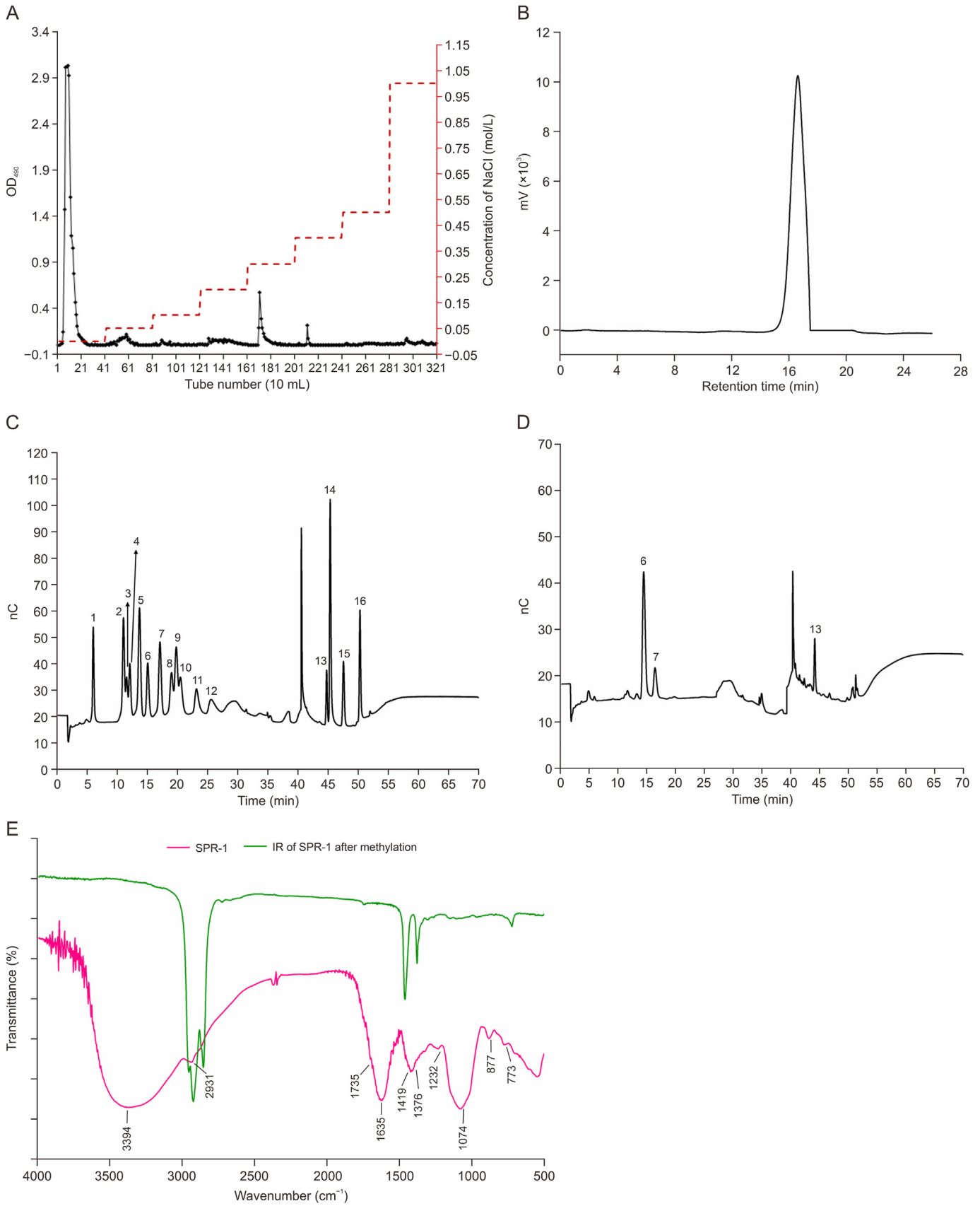

Fig. 1. (A) Elution profile of SPR-1 on DEAE-52 cellulose column. (B) High-performance gel permeation chromatography (HPGPC) of SPR-1. (C) High-performance ion exchange chromatography (HPIEC) of monosaccharide standards and SPR-1. (D) HPIEC of monosaccharide SPR-1. (E) Fourier-transform infrared (FT-IR) spectrum of SPR-1. 1: L-fucose, 2: D-galactosamine hydrochloride, 3: L-rhamnose, 4: D-arabinose, 5: D-glucosamine hydrochloride, 6: D-galactose, 7: D-galactose, 8: *N*-acetyl-D-glucosamine, 9: D-xylose, 10: D-mannose, 11: D-fructose, 12: D-ribose, 13: D-galacturonic acid, 14: L-guluronic acid, 15: D-glucuronic acid, 16: D-mannuronic acid.

with a BRT104-102 column (8 mm × 300 mm, Borui Saccharide, Biotech. Co. Ltd., Yangzhou, China) and a refractive index detector. Based on the reported methodology [34] with slight adaptation, the SPR-1 sample (50 μL) was injected into the HPGPC system and eluted with the mobile phase (0.02% (*m/m*) NaN_3 and 0.1 M $NaNO_3$) with a flow rate of 0.6 mL/min at 35 °C.

2.3.2. Determination of monosaccharide composition

Referring to the previous report [35], the monosaccharide composition of SPR-1 was analyzed using the high-performance ion exchange chromatography (HPIEC) on a Dionex ICS-5000 (Dionex™, Thermo Scientific™, Waltham, MA, USA). In brief, a total of 5.0 mg sample was first hydrolyzed by 2.0 mL TFA solution (3 mol/L) for 3 h at 120 °C. The acid hydrolysis solution was accurately aspirated and transferred to a new tube, blow dry with N_2 blowing and added 5 mL water and mixed well by vertexing. 50 μL above solution was pipetted into a tube and added 950 μL of ultrapure water, and then centrifuged at 12,000 r/min for 5 min. Finally, the sample was analyzed by HPIEC equipped with Dionex Carbopac™ PA20 (3 mm × 150 mm; Dionex™, Thermo Scientific™) and an ICS-6000 DC electrochemical detector (Thermo Scientific™). The conditions are as follows: injection volume: 25 μL; mobile phase A: H_2O; mobile phase B: 15 mM NaOHC:15 mM NaOH and 100 mM NaOAC; rate of mobile phase: 0.3 mL/min; column temperature: 25 °C.

2.3.3. FT-IR spectrometric analysis

The infrared spectra of SPR-1 were recorded in a wavelength range of 4000–400 cm^{-1} on an FT-IR spectrophotometer (Tianjin Port East Science and Technology Development Co., Ltd., Tianjin, China). Briefly, 2 mg of SPR-1 and 200 mg of KBr were accurately weighed and pressed into pellets, and the data were collected using the FT-IR 650.

2.3.4. Methylation analysis

The methylation analysis of SPR-1 was conducted as described previously with slight modifications [36]. Details of the sample preparation procedure are provided in the Supplementary data S1–S2. The acetylated SPR-1 was analyzed by GC-MS instrument (Agilent GC-MS 6890-5973, Agilent, Palo Alto, CA, USA) equipped with an RXI-5 SIL MS column (30 m × 0.25 mm, 0.25 μm). The temperature program was as follows: initial column temperature was 120 °C, and then ramped up from 120 °C at 3 °C/min to 250 °C and maintained at 250 °C for 5 min. The injector and flame ionization detector temperatures were 250 °C. The inlet temperature was 250 °C and the detector temperature was 250 °C/min. The carrier gas was helium (purity, 99.999%) with a flow rate of 1.0 mL/min.

2.3.5. NMR spectroscopy analysis

To allow sufficient exchange of active hydrogen with tritium, the purified SPR-1 powder (50 mg) was dissolved in 0.5 mL of D_2O and freeze-dried. The freeze-dried powder was then re-dissolved in 0.5 mL of D_2O and continued to be freeze-dried again; this process was repeated several times. The Bruker Ascend 600 spectrometer (Bruker, Billerica, MA, USA) at 600 MHz was used to record the one-dimensional (^1H, ^{13}C, and DEPT-135) and two-dimensional (^1H-^1H COSY, HSQC, HMBC and NOESY) NMR spectra of SPR-1.

2.3.6. Surface morphology

The surfaces of the polysaccharide samples were observed using an ultra-high resolution scanning electron microscope (Nova NanoSEM 450, FEI Inc., Hillsboro, OR, USA) and photographed at different magnifications. The details of the sample preparation procedure are provided in the Supplementary data S3.

2.4. Immunomodulatory activity in vitro of SPR-1

2.4.1. Cell culture

The macrophage RAW264.7 cells were cultured in Dulbecco's modified Eagle medium (DMEM) supplemented with 10% fetal bovine serum (FBS) and 1% antibiotic-antimycotic solution at 37 °C and 5% CO_2 under humidified conditions in a cell incubator with a previously documented method [37]. Cells were adjusted to the density of 2 × 10^4 cells/well and inoculated onto 96-well plates overnight, followed by treatment with different concentrations of SPR-1 (0–3000 μg/mL) for 24 h at 37 °C. Following treatment, 3-(4,5-dimethylthiazol-2-yl)-2,5-diphenyltetrazolium bromide (MTT) solution (20 μL, 5 mg/mL) was added to each well and incubated for 4 h. Subsequently, the medium was removed and added in 100 μL dimethyl sulfoxide (DMSO), and the optical density was measured (570 nm) by a multifunction microplate reader (Spark 20 M, Tecan, Mannedorf, Switzerland).

2.4.2. Cytokine assay

The macrophages RAW264.7 cells were seeded into 6-well plates at the density of 1 × 10^5 cells/well and cultured in a humidified incubator at 37 °C and 5% CO_2. After 24 h of incubation, a series of concentrations of SPR-1 (12, 24 and 48 μg/mL) and LPS (positive control, 1 μg/mL) were added to different wells and incubated for another 24 h. At the end of the incubation, the cell culture supernatants were collected for further analysis of the secreted cytokines and stored at −20 °C. According to the instructions of the manufacturers, the levels of NO, IL-1β and TNF-α in macrophage culture media were determined by ELISA kits.

2.4.3. Quantitative real-time polymerase chain reaction (qRT-PCR)

The expression of TNF-α and its relevant genes in macrophages was analyzed by qRT-PCR and referred to a previous report [5]. According to the manufacturer's protocol, the total RNA of each sample was extracted with Trizol reagent (Invitrogen, Carlsbad, CA, USA) and subsequently transcribed into cDNA with the reverse first-strand DNA synthesis kit (TRANSGEN, Beijing, China). qRT-PCR was performed by ViiA™ 7 real-time PCR system (Applied Biosystems, Grand Island, NY, USA) within the FastStart Universal SYBR-Green Master Rox (Roche Diagnostics, Indianapolis, IN, USA) following the manufacturer's instructions. The reaction mixture (10 μL) contained 1 μL of the cDNA template, 0.4 μL of each primer (10 nmol/L, 0.2 μL of each 5′ upstream and 3′ downstream primer), 5 μL of the SYBR qPCR mix, and 3.6 μL of RNase-free water. PCR primers were synthesized by Sangon Biotech (Shanghai, China), and the primer sequences used for qRT-PCR are listed in Table S1. The PCR cycling parameters included 50 °C for 10 min followed by 95 °C for 10 min, and then 40 cycles of 95 °C for 15 s and 60 °C for 1 min. The relative gene expression of each gene was determined with the $2^{-\Delta\Delta Ct}$ method, using the reference genes (*GAPDH*) as a normalized gene.

2.5. The predictive interaction of SPR-1 and LPS with MD2

2.5.1. ITC analysis of SPR-1 and LPS interactions with MD2

The binding affinity of SPR-1 or LPS to MD2 was measured directly by PEAQ-ITC (Malvern Panalytical, Worcestershire, UK). In brief, SPR-1 or LPS was diluted to 20 μM and MD2 protein was diluted to 2 μM by phosphate buffered saline (PBS) buffer (pH 7.4). In the experiment, a solution of SPR-1 or LPS was loaded into the syringe of the ITC apparatus and an MD2 protein solution was in the calorimetric cell. During each ITC experiment, 13 injections of SPR-1 or LPS into the calorimetric cell were carried out. The duration of each injection was 150 s. The stirring speed was 750 r/min. The detection temperature was 25 °C. At the same time, to exclude the

heat background, the ligand and MD2 were dropped into the buffer at the same concentration under the same conditions.

2.5.2. Molecular docking of SPR-1 and LPS with MD2

The crystal structure of MD2 (PDB: 4G8A) was downloaded from Protein Data Bank (https://www.rcsb.org/). The protein structure was used as the initial structure for subsequent molecular docking. The initial structure was processed with AutoDock Tools 1.5.6 to add the polar hydrogen atoms and Gasteiger charges and generate a pdbqt file for docking [38,39]. The 3D structures of SPR-1 and LPS were drawn using Chem3D software, and then saved in mol2 format. In general, the most commonly used docking method for large molecules is the semi-empirical optimization method; and some researchers have used the Parameterized Model 3 (PM3) semi-empirical optimization method to study cyclodextrin [40]. Therefore, we used the PM3 semi-empirical calculation method for SPR-1 and LPS. The molecular structures were optimized using the MOPAC program and PM3 atomic charges were calculated for subsequent molecular docking, and the ligand structures were processed using AutoDock Tools 1.5.6 to generate pdbqt files for docking [41]. Molecular docking of SPR-1 and LPS with MD2 were performed using AutoDock 4.2 software via the Lamarckian genetic algorithm. The number of grid points in the XYZ of the grid box was set to $80 \times 80 \times 80$, the number of docking times was set to 50, and the rest of the parameters were used as default values. In order to mitigate the potential impact of unreasonable atomic contacts in the structural space resulting from molecular docking, an energy optimization method can be employed to obtain a structurally stable model [42]. The energy optimization was performed using the Amber14 force field, and the optimization process was carried out in two steps: a 1000-step steepest descent method optimization, followed by a 500-step conjugate gradient method for further optimization of the structure, and the final result was used as a model for subsequent analysis.

2.6. Data analysis

Data were analyzed using GraphPad Prism 9.5 and all results were expressed as mean ± standard error of mean (SEM). Dunnett's test of one-way analysis of variance (ANOVA) was used to analyze the difference between three or more groups. A significant difference was statistically set as $P < 0.05$ or $P < 0.01$.

3. Results and discussion

3.1. Characterization of SPR-1

3.1.1. Determination of homogeneity and molecular mass

The HPGPC spectrum of SPR-1 showed a single symmetrical and narrow peak (Fig. 1B), indicating that SPR-1 was a homogeneous polysaccharide. The yield of SPR-1 was 3.38%. According to the HPGPC result, the weight average molecular weight (Mw) and the number average molecular weight (Mn) of SPR-1 were found to be 3,622 Da and 2,289 Da, respectively, and the polydispersity (Mw/Mn) value was 1.58. Significantly, according to many research, molecules with low polydispersity mean that these molecules are homogeneously dispersed in aqueous solution and do not form large aggregates; the polymers with polydispersity ratios closer to 1, the narrower the molecular weight distribution [43,44]. Consequently, the above analysis presumes that the structural features of SPR-1 had a narrow molecular weight distribution and a simple branched chain structure.

3.1.2. Monosaccharide composition determination

The results of the HPIEC of 16 standards and SPR-1 are shown in Figs. 1C and D. The SPR-1 was composed of Gal (61.9%), Glc (27.5%) and GalA (10.6%), indicating that SPR-1 was an acidic polysaccharide. This result differed from previous reports. Previous studies showed that the polysaccharides from PR were rich in Fru [2,18,45]. In addition, the higher Gal content in SPR-1 may be due to the steaming process [46]. It was shown that during the isolation and purification of polysaccharides with DEAE-52, the content of Glc, Gal and Man gradually decreased with the gradual increase of salt concentration in the eluate, while SPR-1 was eluted using pure water, which may also account for the fact that SPR-1 was mainly composed of Gal [47].

3.1.3. FT-IR analysis of SPR-1

The FT-IR spectra properties of SPR-1 displayed typical polysaccharide absorption peaks (Fig. 1E). In particular, the strong and broad absorption peak between 3600 and 3200 cm^{-1} could be observed, which attributed to the O—H stretching vibration of hydroxyl groups. The relatively strong absorption peak at 2931 cm^{-1} was attributed to the stretching vibration of the C—H bond in CH_2 or CH_3 [48]. The peaks at 1735 cm^{-1} and 1635 cm^{-1} were attributed to the methyl-esterified carbonyl groups (COO—CH_3) and the carboxylate ion (COO^-) stretching band, respectively, which proved the presence of uronic acid in SPR-1 [49,50]. The absorption peak at 1419 cm^{-1} was related to the C—O stretching vibration [51]. An absorption peak at 1376 cm^{-1} was attributed to the C═O symmetric stretching vibration [52]. The absorption peaks at 1232 cm^{-1} and 1074 cm^{-1} were ascribed to O—H variable angle vibration [53]. The absorption peak at 877 cm^{-1} was related to the C—H angular vibration of the equatorial bond other than the C—H isomerization of the terminal group of the pyran ring. The absorption peak detected at 773 cm^{-1} was attributable to the telescopic vibration of the symmetrical ring of the pyran ring. Therefore, these results further verified that β-D-Gal was the main component of SPR-1.

3.1.4. Methylation analysis

Methylation analysis is one of the most effective and commonly used method to identify the linkage types and their proportions in polysaccharides [5]. To determine the glycosidic bond of SPR-1, methylation was conducted and the total ion chromatograms (TIC) of PMAAs from SPR-1 were studied. The TIC chromatogram was shown in Fig. S3. GC-MS analysis showed that the SPR-1 consisted of 8 PMAAs. Table 1 shows these 8 PMAAs, containing their corresponding glycosidic linkages and molar ratios. Fig. S3 presents the representative ionization and mass spectra of 8 PMAAs, based on the databases of GC-EIMS of PMAAs (Complex Carbohydrate Research Center, University of Georgia, USA) and data previously reported in the kinds of literature [54,55]. As seen in Table 1, the PMAA derivatives of SPR-1 were measured to be 2,3,4,6-Me_4-Glc*p*, 2,3,4,6-Me_4-Gal*p*, 2,4,6-Me_3-Gal*p*, 2,3,6-Me_3-Gal*p*, 2,3,6-Me_3-Glc*p*, 2,3,4-Me_3-Glc*p*, 2,3-Me_2-Glc*p* and 2,3-Me_2-Gal*p* with the molar of 4.0:3.8:5.7:59.7:11.0:7.1:3.5:6.6. Besides, after uronic acid reduction, the content of Gal increased indicating the presence of →4)-Gal*p*A-(1→ [56]. The results indicated that SPR-1 mainly consisted of 1,4-linked Gal*p*A fragment, 1,4-linked Gal*p* fragment and 1,4-linked Glc*p* fragment. The structural features could be further verified and explained in detail with NMR.

3.1.5. NMR spectrum analysis

Currently, NMR spectroscopy is a common and effective method for analyzing the structural characteristics of polysaccharides. The configuration and amount of sugar residues in polysaccharides could be determined with ^1H and ^{13}C spectra according to their chemical shift and coupling constant, and the sequences of the sugar residues could be defined by NOESY and HMBC spectrums [57—59]. Hence, we investigated the ^1H, ^{13}C, COSY, HSQC, HMBC and

Table 1
Methylation analysis of SPR-1.

No.	Retention time (min)	Methylated sugar	Mass fragments (m/z)	Molar ratio	Type of linkage
1	16.953	2,3,4,6-Me_4-Glc*p*	43,71,87,101,117,129,145,161,205	4.0	Glc*p*-(1→
2	17.887	2,3,4,6-Me_4-Gal*p*	43,71,87,101,117,129,145,161,205	3.8	Gal*p*-(1→
3	21.055	2,4,6-Me_3-Gal*p*	43,87,99,101,117,129,161,173,233	5.7	→3)-Gal*p*-(1→
4	21.393	2,3,6-Me_3-Gal*p*	43,87,99,101,113,117,129,131,161,173,233	59.7	→4)-Gal*p*-(1→/→4)-GalpA-(1→[a]
5	21.802	2,3,6-Me_3-Glc*p*	43,87,99,101,113,117,129,131,161,173,233	11.0	→4)-Glc*p*-(1→
6	22.16	2,3,4-Me_3-Glc*p*	43,87,99,101,117,129,161,189,233	7.1	→6)-Glc*p*-(1→
7	26.679	2,3-Me_2-Glc*p*	43,71,85,87,99,101,117,127,159,161,201	3.5	→4,6)-Glc*p*-(1→
8	27.088	2,3-Me_2-Gal*p*	43,71,85,87,99,101,117,127,159,161,201,261	6.6	→4,6)-Gal*p*-(1→

Glc: glucose; Gal: galactose; GalA: galacturonic acid; *p*: pyranose.
[a] Dominate percentage in the mixture of →4)-Gal*p*-(1→ and →4)-Gal*p*A-(1→.

NOESY NMR spectra of SPR-1 at 600-MHz. The C/H chemical shifts of all monosaccharide residues (A-M) were assigned and are listed in Table 2 according to the literature and in combination with Fig. 2. The majority of the proton and carbon signals of SPR-1, with chemical shifts ranging from 3.00 to 5.50 ppm and 60–120 ppm, respectively, were the signature signals of polysaccharide, as shown in Figs. 2A and B [35,60]. In the ^{1}H NMR spectrum, the anomeric proton region (5.50–4.30 ppm) had 12 main signals at 5.31, 5.26, 5.15, 4.91, 4.88, 4.88, 4.83, 4.57, 4.56, 4.55, 4.51 and 4.35 ppm, indicating that SPR-1 contained 12 residues (named F, H, J, I, G, L, M, K, A, E, D and B residues). Meanwhile, the signals at 3.2–4.0 ppm were assigned to protons in the sugar ring. In the ^{13}C NMR (150 MHz, D_2O) spectra, nuclear magnetic carbon spectrum signals were mainly concentrated between 60 and 120 ppm. The ^{13}C NMR spectrum showed anomeric carbon signals at 105.90, 105.78, 105.39, 105.09, 101.75, 101.34, 101.33, 100.89, 99.89, 99.10, 97.01 and 93.33 ppm, which corresponded to the C1 of residues A, D, E, B, L, M, H, F, G, I, K and J, respectively. The Dept135 spectrum (Fig. S4) showed that the inverted peaks 68.46, 66.80, 65.04, 63.61, 63.51, 62.65, 62.35, 62.20, 61.92 and 61.89 ppm were assigned to C6. The resonance signals of anomeric proton at 4.4–5.3 ppm and anomeric carbon at 90–110 ppm confirmed the presence of both α- (4.9–5.3) and β-configuration (4.4–4.9) in SPR-1, which verified the results of IR spectroscopy [61,62]. Further evidence for the presence of the carboxyl carbon of Gal*p*A was found at the 170–176 ppm signals in the ^{13}C NMR spectrum based on the monosaccharide composition and methylation analysis [55].

The anomeric chemical shifts at 4.56/105.90 ppm indicated that residue A was in the β-configuration. The COSY spectrum showed that the chemical ships observed at 4.56, 3.60, 3.69 and 4.08 ppm were assigned for H1, H2, H3 and H4, respectively, while chemical shifts corresponding to C1, C2, C3, C4 and C6 appeared at 105.90, 73.31, 74.94, 79.13 and 62.20 ppm from HSQC, respectively. The anomeric chemical shifts at 4.51/105.78 ppm indicated that residue D was in the β-configuration. The COSY spectrum showed that the chemical ships observed at 4.51, 3.47, 3.62 and 4.07 ppm were assigned for H1, H2, H3 and H4, respectively, while chemical shifts corresponding to C1, C2, C3, C4 and C6 appeared at 105.78, 72.31, 69.27, 79.38 and 65.04 ppm from HSQC, respectively. The complete ^{1}H and ^{13}C chemical shifts for residues A and D are listed in Table 2. Therefore, a comparison of the experimental proton and carbon resonances with the dates from the literature [9,54] allowed assigning residue A and D to →4)-β-D-Gal*p*-(1→ and →4,6)-β-D-Gal*p*-(1→, respectively.

The anomeric chemical shift of residue B was 4.35/105.09 ppm, suggesting that residue B was in the β-configuration. The COSY spectrum showed that the chemical shift of H1-2 was 4.35/3.42, the chemical shift of H2-3 was 3.42/3.55, and the chemical shift of H4-5 was 4.03/3.84. We could deduce that H1, H2 H3, H4 and H5 were 4.35, 3.42, 3.55, 4.03 and 3.84 ppm, respectively, while chemical

Table 2
Chemical shift assignments of SPR-1.

Symbol	Glycosyl residues	H1/C1	H2/C2	H3/C3	H4/C4	H5/C5	H6a/C6	H6b	$COOCH_3$	O_2CCH_3
A	→4)-β-D-Gal*p*-(1→	4.56	3.60	3.69	4.08	3.63	3.76	3.65		
		105.90	73.31	74.94	79.13	76.11	62.20			
B	β-D-Gal*p*-(1→	4.35	3.42	3.55	4.03	3.84	3.76	3.65		
		105.09	72.35	73.93	71.46	74.89	61.92			
D	→4,6)-β-D-Gal*p*-(1→	4.51	3.47	3.62	4.07	3.61	3.46	3.94		
		105.78	72.31	69.27	79.38	76.11	65.04			
E	→3)-β-D-Gal*p*-(1→	4.55	3.58	3.68	4.12	3.93	3.85	3.75		
		105.39	72.1	79.17	69.74	74.9	62.35			
F	→4)-α-D-Glc*p*-(1→	5.31	3.55	3.90	3.58	3.78	3.78	3.71		
		100.89	72.91	74.56	78.31	72.53	61.89			
G	→4,6)-α-D-Glc*p*-(1→	4.88	3.49	3.67	3.56	3.57	3.78	3.89		
		99.89	72.86	74.02	77.10	70.69	68.46			
H	α-D-Glc*p*-1→	5.26	3.60	3.70	3.95	3.97	3.60	3.82		
		101.33	71.94	74.03	70.61	71.68	62.65			
I	→6)-α-D-Glc*p*-(1→	4.91	3.53	3.67	3.47	3.86	3.70	3.93		
		99.10	72.73	74.63	70.87	71.47	66.80			
J	→4)-α-D-Glc*p*	5.15	3.48	3.90	3.55	3.77	3.58	3.51		
		93.33	72.80	77.40	79.52	72.11	63.51			
K	→4)-β-D-Glc*p*	4.57	3.19	3.70	3.77	3.58	3.58	3.51		
		97.01	75.56	77.50	78.39	74.99	63.61			
L	→4)-α-D-GalA*p*-(1→	4.88	3.67	3.93	4.37	5.08			1.96	
		101.75	69.40	70.05	80.88	71.99	176.70		21.79	
M	→4)-α-D-GalA*p*-(1→(OMe)	4.83	4.17	4.09	4.36	3.98		3.73		
		101.34	72.70	78.47	79.62	71.94	171.33	54.13		

Gal: galactose; Glc: glucose; GalA: galacturonic acid; *p*: pyranose; OMe: methoxyl.

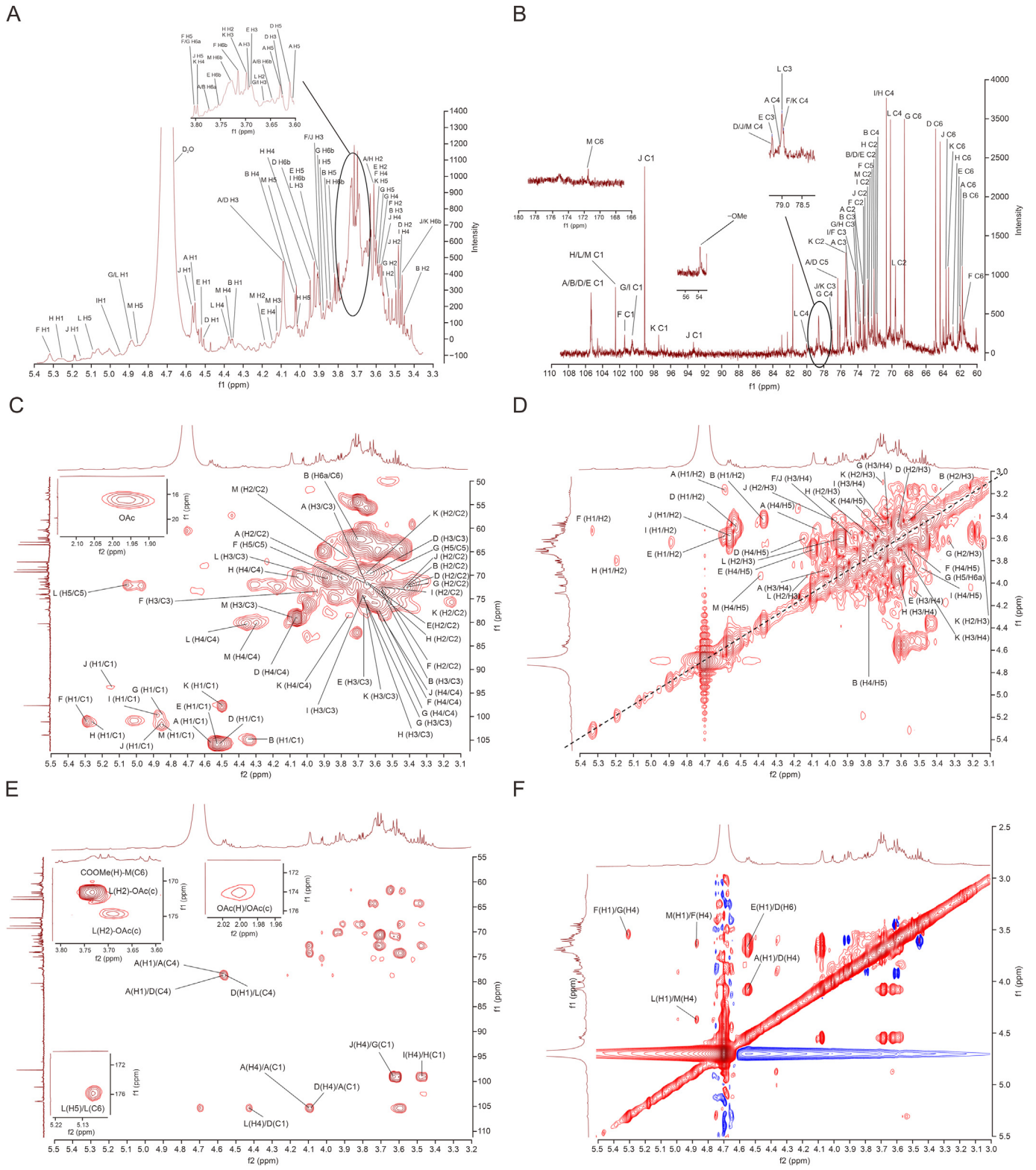

Fig. 2. The nuclear magnetic resonance (NMR) spectra of SPR-1. The (A) ^{1}H NMR, (B) ^{13}C NMR, (C) HSQC, (D) COSY, (E) HMBC, and (F) NOESY spectra of SPR-1.

shifts corresponding to C1, C2 C3, C4 and C5 appeared at 105.09, 72.35, 73.93, 71.46 and 74.89 ppm, respectively. Furthermore, the complete ^{1}H and ^{13}C signals of residue B were consistent with the data previously reported in the literature [9], which confirmed that residue B was β-D-Gal*p*-(1→. Based on the HSQC spectroscopy, the chemical shifts were attributed to H1 and C1 at 4.55/105.39 ppm, indicating that residue E was a β-configuration residue. The chemical shifts of H2 to H6a/b were determined from the COSY spectrum. Consequently, residue E was inferred to be →3)-β-D-Gal*p*- [55].

Since the chemical shifts at 5.31/100.89, 4.88/99.89, 5.26/101.33, 4.91/99.10 and 5.15/93.33 were described as H1 and C1, it was presumed that residues F, G, H, I and J were the α-configuration. The signals from COSY spectra were obtained for H2 to H6a/b. In addition, the matching C chemical shifts were C2 to C5 based on the HSQC spectrum. The complete ^{1}H and ^{13}C chemical shifts for residues F, G, H, I and J were almost consistent with the literature [27,54,63], the proposed unit of residues F, G, H, I and J were →4)-α-D-Glc*p*-(1→, →4,6)-α-Glc*p*-(1→, α-D-Glc*p*-(1→, 6)-α-Glc*p*-(1→, and 4)-α-Glc*p*, respectively. The chemical shifts of residue K at 4.57/97.01 ppm in the HSQC spectroscopy were assigned to H1 and C1, suggesting that residue K was an α-configuration residue. The chemical shifts of residue K at 4.57/97.01 ppm in the HSQC spectroscopy were assigned to H1 and C1, suggesting that residue K was an α-configuration residue. The signals of H2 to H6a/b were determined with the COSY spectrum. Therefore, we presumed that residue K was →4)-β-D-Glc*p* [54].

Based on the previous report [49] and HSQC spectrum, the chemical shift at 54.13 ppm and the signal at 3.73 ppm provided evidence for the presence of a methoxyl ester group in SPR-1. Meanwhile, the presence of the methoxyl ester group was further supported by the 3.73/171.33 ppm chemical shift in the HMBC spectrum. The presence of the acetyl group in SPR-1 was supported by the proton signal at 1.96 ppm in the ^{1}H NMR spectrum and the carbon signals at 21.79 ppm and 176.70 ppm in the ^{13}C NMR spectrum [55]. As previously reported in the literature, the low-field shift of the signal for the proton can be attributed to the de-shielding effect of the electron-withdrawing carbonyl [64], and the H5 signal of residue L was 5.08. Based on HSQC and COSY, the signals of residue L were H1/C1 (4.88/101.75), H2/C2 (3.67/69.40), H3/C3 (3.93/70.05), H4/C4 (4.37/80.88), and H5/C5 (5.08/71.99). And then, as shown in HMBC, the 1.96/174.09 ppm and 3.69/175.25 ppm signals, and the peaks at 1.96/21.79 ppm and 3.67/69.40 (LH2/LC2) ppm in the HSQC spectrum revealed that the acetyl group was linked to a carbon with a chemical shift of 69.40 ppm, which was C2 chemical shift of residue L. Based on HSQC and COSY, the signals of residue M were H1/C1 (4.83/101.34), H2/C2 (4.17/72.70), H3/C3 (4.09/78.47), and H4/C4 (4.36/79.62). As shown in HMBC, the residue M indicated that the H5 protons (3.98 ppm) made intra-residue contact with the carboxyl carbon at 171.33 ppm (C6) and further connected with the protons of the methoxyl group (3.73 ppm) with C6 (171.33 ppm) [55]. Therefore, the chemical shifts of 176.70 ppm and 171.33 ppm were the signals of the C6 of the unesterified and esterified D-Gal*p*A units, respectively. The complete ^{1}H and ^{13}C chemical shifts for residues L and M were listed in Table 2, and were nearly consistent with those reported in

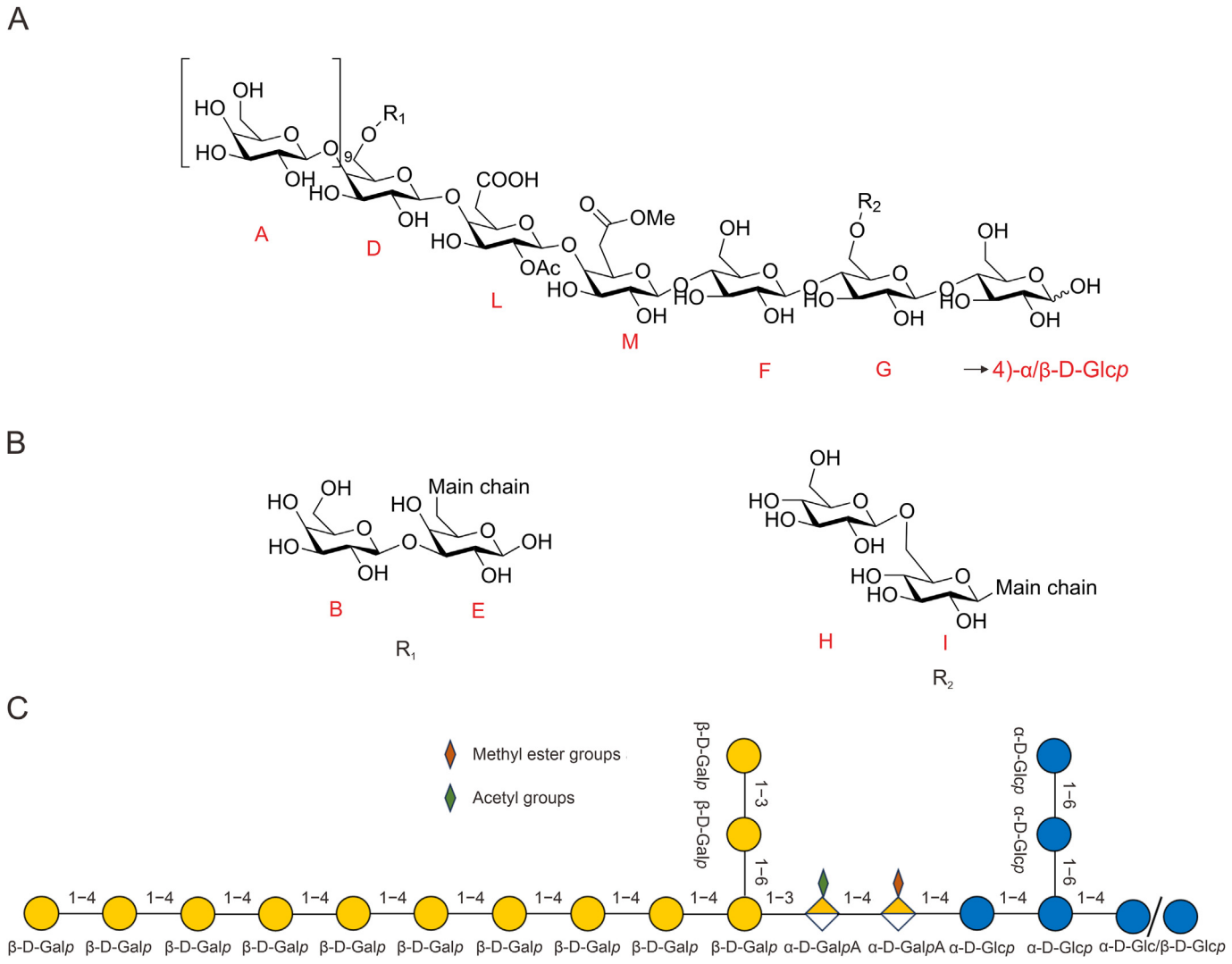

Fig. 3. The (A) main chain, (B) branched-chain, and (C) hypothetical structure model of SPR-1.

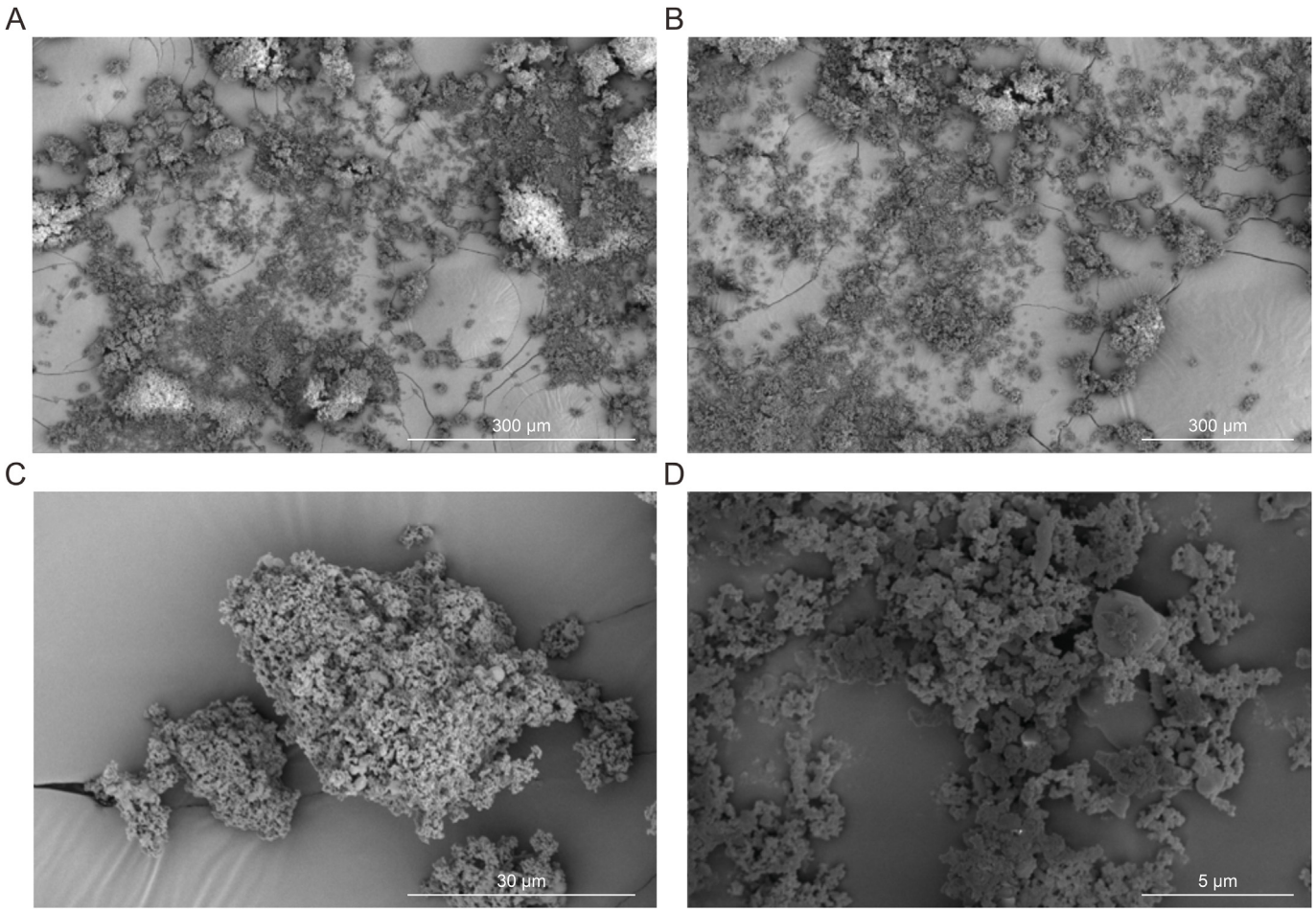

Fig. 4. The scanning electron microscope (SEM) of SPR-1.

the literature [65,66], while the downfield resonances of the C4 at 80.88/79.62 ppm for residue L and residue M confirmed that residues L and M were →4)-α-2-O-ace-Gal*p*A-(1→, and →4)-α-Gal*p*A-(1→(OMe), respectively.

HMBC analysis showed that the H1 and C1 of the →4)-β-D-Gal*p*-(1→ has a correlation peak with its own C4 and H4, suggesting the presence of →4)-β-D-Gal*p*-(1 → 4)-β-D-Gal*p*-(1→ glycosidic bond. The H1 and C1 of the →4)- β-D-Gal*p*-(1→ has a correlation peak with C4 and H4 of the →4,6)-β-D-Gal*p*-(1→, suggesting the existence of a →4)-β-D-Gal*p*-(1 → 4,6)-β-D-Gal*p*-(1→ linkage. In addition, the H1 and C1 of →4,6)-β-D-Gal*p*-(1→ has related peaks to C4 and H4 from →4)-α-D-Gal*p*A-(1→, which indicated the presence of a →4,6)-β-D-Gal*p*-(1 → 4)-α-D-Gal*p*A-(1→ linkage.

The correlation peak in the NOESY between the H1 of →4)-α-D-Gal*p*A-(1→ and the H4 of →4)-α-D-Gal*p*A-(1→(OMe) suggests that the presence of the glycosidic bond →4)-α-D-Gal*p*A-(1 → 4)-α-D-Gal*p*A-(1→(OMe). Meanwhile, the correlation peak between the H1 of →4)-α-D-Gal*p*A-(1→(OMe) and the H4 of →4)-α-D-Glc*p*-(1→ suggests that the presence of the glycosidic bond →4)-α-D-Gal*p*A-(1→(OMe)→4)-α-D-Glc*p*-(1→, and the H1 of the →4)-α-D-Glc*p*-(1→ has a correlation peak with H4 of the →4,6)-α-D-Glc*p*-(1→, indicating the existence of a →4)-α-D-Glc*p*-(1 → 4,6)-α-D-Glc*p*-(1→ linkage. The NOESY spectrum showed that the H1 of the →3)-β-D-Gal*p*-(1→ has a correlation peak with H6 of the →4,6)-β-D-Gal*p*-(1→, indicating the existence of →3)-β-D-Gal*p*-(1 → 4,6)-β-D-Gal*p*-(1→ glycosidic bond. The correlation peak between the H1 of →4)-α-D-Glc*p*-(1→ and the H4 of →4,6)-β-D-Glc*p*-(1→ suggests the presence of the glycosidic bond →4)-α-D-Glc*p*-(1 → 4,6)-β-D-Glc*p*-(1→. In addition, the H1 of →6)-α-D-Glc*p*-(1→ has related peaks to H6 from →4,6)-α-D-Glc*p*-(1, indicating the presence of a →4)-α-D-Glc*p*-(1 → 4,6)-α-D-Glc*p*-(1→linkage. The HMBC and NOESY correlations of the glycosidic bonds of SPR-1 are shown in Table S2.

Hence, combining the above analysis we presumed that the connection of the main chain was →[4)-β-D-Gal*p*-(1]$_9$ → 4,6)-β-D-Gal*p*-(1 → 4)-α-D-Gal*p*A-(1 → 4)-α-D-Gal*p*A-(1 → 4)-α-D-Glc*p*-(1 → 4,6)-α-D-Glc*p*-(1 → 4)-α/β-D-Glc*p*, and the connection of the branch chains were R_1: β-D-Gal*p*-(1 → 3)-β-D-Gal*p*-(1→ and R_2: α-D-Glc*p*-(1 → 6)-α-D-Glc*p*-(1→. A schematic diagram of the predicted partial structure of SPR-1 is shown in Fig. 3.

3.1.6. SEM

The surface topographies of SPR-1 were observed by SEM at the magnitude of 300 μm (500×), 100 μm (1,000×), 30 μm (5,000×) and 5 μm (20,000×) scale. As can be seen from Figs. 4A and B, the polysaccharide structure appeared fragmented at 500× and 1,000× magnification and had a rough surface, which may be caused by various hydroxyl and carboxyl groups [67]. Under the 5,000× and 20,000× microscope (Figs. 4C and D), the polysaccharide showed a honeycomb shape with numerous irregular bumps.

3.2. Immunomodulatory activity in vitro of SPR-1

3.2.1. Effect of SPR-1 on the RAW264.7 cells viability

The inhibitory effect of SPR-1 polysaccharide on RAW264.7 cell growth was assessed using MTT assays. As shown in Fig. 5A, SPR-1

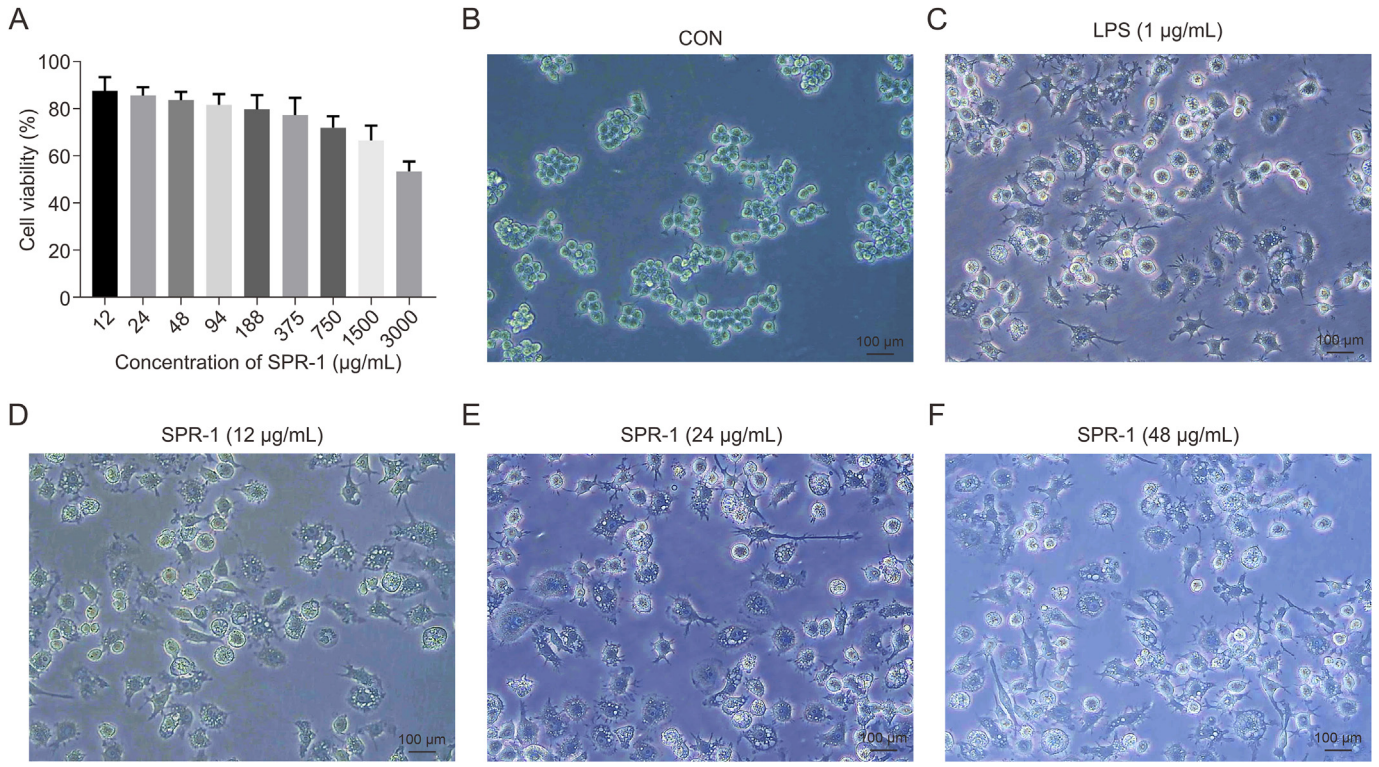

Fig. 5. (A) The cell viability of RAW264.7 cells was assessed by 3-(4,5-dimethylthiazol-2-yl)-2,5-diphenyltetrazolium bromide (MTT) assay. (B–F) The effects of different concentrations of SPR-1 (12, 24 and 48 μg/mL) on the morphology of RAW264.7 cells. LPS: lipopolysaccharide; CON: control.

could decrease the survival rate of RAW264.7 cells in a dose-dependent manner. Based on the experimental results, three concentrations of 12, 24 and 48 (μg/mL), which had almost no significant effect on cell survival, were selected for subsequent experiments.

3.2.2. Morphological observation of macrophages

As shown in Figs. 5B–F, RAW264.7 cells in the control group were round, respectively, and had smooth and intact cell walls. After 24 h of LPS treatment, compared with the control group, RAW 264.7 cells in the LPS group were adhered, swollen, and their volume increased with an irregular shape, which formed a slender pseudopod. The SPR-1 group also showed morphological changes similar to those in the LPS group, which indicated that both LPS and SPR-1 could activate RAW264.7 cells and induce morphological changes and activate immune activity. Fig. 6A demonstrates activation index of RAW264.7 cells by LPS and SPR-1 (12, 24 and 48 μg/mL).

3.2.3. SPR-1 polysaccharide regulated the production of inflammatory mediators in RAW264.7

While immune cells were stimulated by exogenous stimulants, immune cells secreted cytokines (e.g., NO, IL-1β, and TNF-α) to stimulate the immune response of immune cells. Therefore, NO, TNF-α and IL-1β can be considered to be a quantifier of the immune cells' activation. In the current study, the immunomodulatory activities of macrophages treated with LPS and SPR-1 were assessed by measuring the secretion of NO, IL-1β and TNF-α (Figs. 6B–D). Compared to the control group, the concentration of NO in macrophages treated with LPS and SPR-1 was significantly increased ($P < 0.001$); however, the concentration of NO was not dose-dependent with SPR-1 dose. When the concentration of SPR-1 was 24 μg/mL, the ability of macrophages to induce NO was essentially equated to the LPS group. Thus, LPS and SPR-1 could significantly increase the ability to induce NO. Compared to the control group, the different concentrations of SPR-1 significantly increased the concentration of IL-1β, and the difference was statistically significant compared with the control group ($P < 0.01$), and the increase was dose-dependent. Compared to the LPS group, different concentrations of SPR-1 from 12 to 48 μg/mL were statistically significant ($P < 0.05$). The secretion of TNF-α in RAW264.7 cells treated with LPS and different concentrations of SPR-1 were statistically significant ($P < 0.001$). The different concentrations of SPR-1 induced the secretion of TNF-α in macrophages with almost the same intensity of action. LPS was a potent stimulator for macrophages and could enhance cytokine production in macrophages even at low concentrations. In our study, we compared the effects of direct stimulation of SPR-1 with LPS (1 μg/mL) on RAW264.7 cells. The results showed that SPR-1 and LPS both could promote the production of cytokines (i.e., NO, IL-1β and TNF-α). Therefore, there was a conclusion that SPR-1 could increase the secretion of immunomodulatory factors of macrophage *in vitro*, and its functions were similar to LPS. Our study had similar properties which had been identified in previous studies about alfalfa polysaccharides [68].

3.2.4. Effects of SPR-1 on cytokine mRNA expression in RAW264.7 macrophages

To further study the mechanisms underlying the striking increase in cytokine release, we measured the gene expression of these mediators in RAW264.7 cells by reverse transcription-quantitative polymerase chain reaction (RT-qPCR) (Figs. 6E–H). The mRNA expression levels of the nitric oxide synthase (iNOS) in LPS and SPR-1 (48 μg/mL) treated cells were significantly upregulated ($P < 0.001$) compared to the control group, while the difference in the iNOS expression levels between SPR-1 (12 and 24 μg/

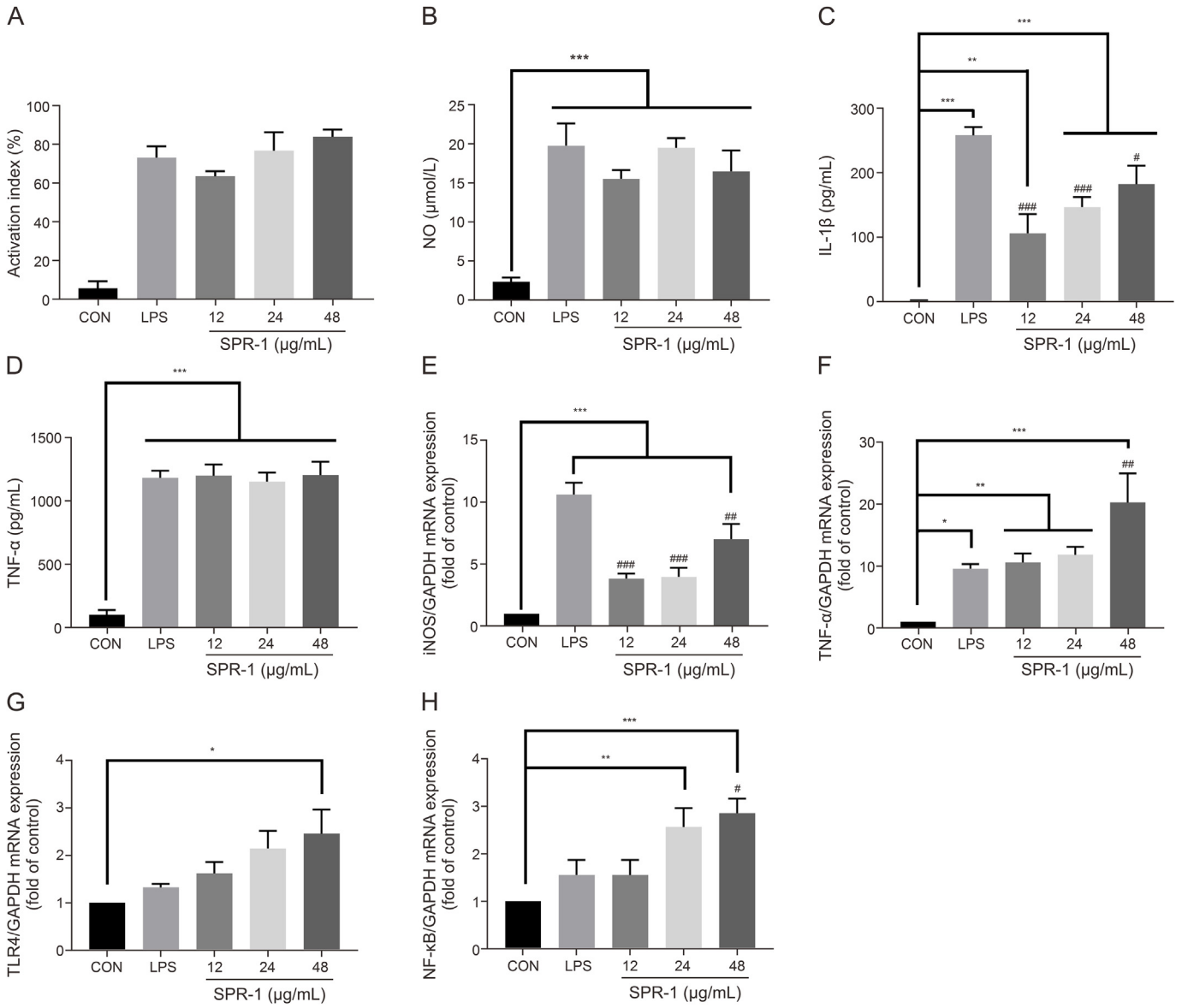

Fig. 6. (A) The activation index of RAW264.7 cells. (B) NO, (C) interleukin-1beta (IL-1β) and (D) tumour necrosis factor alpha (TNF-α) secretion of RAW264.7. The effects of SPR-1 on the expression of (E) nitric oxide synthase (iNOS), (F) TNF-α, (G) Toll-like receptor 4 (TLR4), and (H) nuclear factor-kappa-B (NF-κB) genes in RAW264.7 macrophages. The gene expression was normalized to glyceraldehyde-3-phosphate dehydrogenase (GAPDH). All data are represented as the mean ± standard error of mean (SEM) ($n = 6$). $^{*}P < 0.05$, $^{**}P < 0.01$ and $^{***}P < 0.001$ compared with the control group, $^{\#}P < 0.05$, $^{\#\#}P < 0.01$ and $^{\#\#\#}P < 0.001$ compared with the lipopolysaccharide (LPS) group. CON: control.

mL) was not significant ($P > 0.05$). The relative expression level of the iNOS gene was significantly inhibited ($P < 0.01$) by SPR-1 in a dose-dependent manner compared with the LPS group, but with lower strength. These findings could well explain the roles of SPR-1 in promoting cytokine secretion and NO production. LPS significantly increased the levels of TNF-α cytokines in comparison with the control group ($P < 0.05$). Concurrently, we revealed that SPR-1 had a higher intensity and dose-dependent manner on the relative expression level of the TNF-α gene compared to the LPS group. On the contrary, there was no significant difference in the relative expression levels of Toll-like receptor 4 (TLR4) genes ($P > 0.05$), although the cells treated with SPR-1 were dose-dependently increased compared with the LPS and the control group. We found that SPR-1 had a higher intensity and dose-dependent manner on the relative expression level of the nuclear factor-kappa-B (NF-κB) gene when compared to the LPS group. The relative expression level of the NF-κB gene significantly increased ($P < 0.01$) in cells treated with SPR-1 (24 and 48 μg/mL) compared with the LPS and control group. Therefore, there was a conclusion that SPR-1 could promote the secretion of gene expression of macrophage cells in vitro, and the functions of SPR-1 were similar to LPS. Meanwhile, these results suggest that SPR-1 may play a role in macrophage activation through TLR4 and NF-κB signaling pathways.

Furthermore, because of the interactions of polysaccharides with immunological cell membrane receptors, several studies have reported that the relationship between structural features and bioactivities of function has indicated that a number of polysaccharides linked by β-(1 → 6) glycosidic bonds or consisted of β-(1 → 3)-Glc residues might be suggested as prospective potential immune activators [69]. This may explain the immunomodulatory activity of SPR-1 containing β-(1 → 3)-D-Glc residues. The study showed that polysaccharides with richer Gal of monosaccharide composition could exhibit stronger immunomodulatory activity

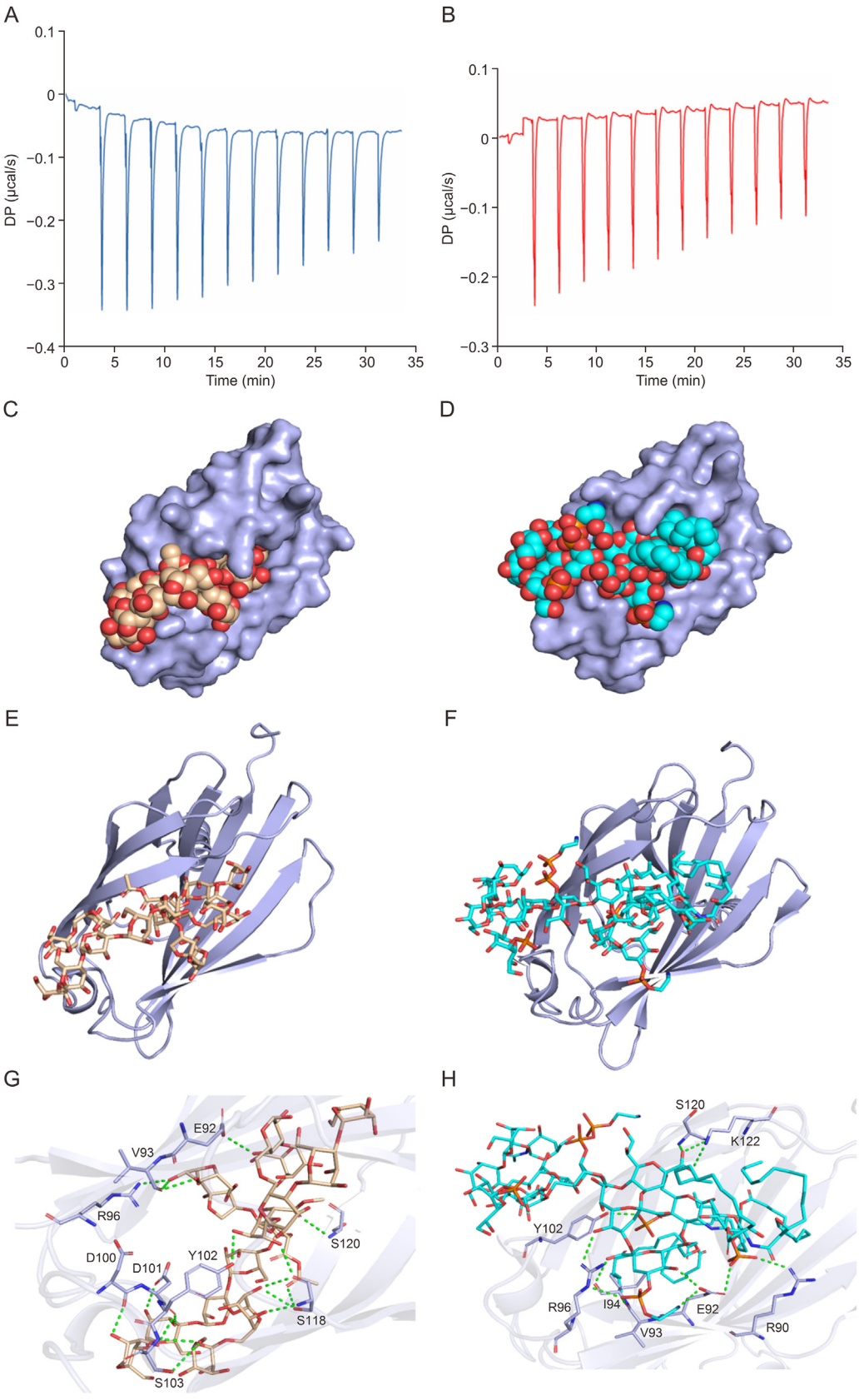

Fig. 7. Isothermal titration calorimetry (ITC) analysis and molecular docking results. (A) ITC analysis showing the binding of SPR-1 to MD2. (B) ITC analysis showing the binding of lipopolysaccharide (LPS) to MD2. (C) Distribution of SPR-1 on the surface of MD2 surface.(D) Distribution of LPS on the surface of MD2 surface. (E) Spatial location of SPR-1 in MD2. (F) Spatial location of LPS in MD2. (G) 3D interaction diagram of SPR-1 with MD2. (H) 3D interaction diagram of LPS with MD2.

[4]. This may explain the immunomodulatory activity of SPR-1 containing large amounts of Gal.

3.3. The predictive interaction of SPR-1 and LPS with MD2

3.3.1. Detection of SPR-1 and LPS interactions with MD2

Previous studies have shown that polysaccharides may activate TLR4 signaling pathways, causing immunomodulatory effects [70]. Notably, polysaccharides can be recognized by the TLR4, resulting in immune responses. MD2 is an essential coreceptor component of TLR4. TLR4 signaling is dependent on the coreceptors MD2 and CD14 binding ligands. When MD2 binds to polysaccharides, it promotes the TLR4/MD2 complex to form a heterodimer, which leads to following downstream signaling [71]. The ITC analysis results provided relevant information on the interaction of SPR-1 or LPS with MD2 protein. As shown in Figs. 7A and B, both SPR-1 and LPS could bind with MD2, and the binding curves and thermodynamic profile for SPR-1 and LPS with MD2 were shown in Table S3 and Fig. S5. Monitor changes in the thermodynamic parameters by ITC revealed that both SPR-1 and LPS binding to MD2 was spontaneous with Gibbs free energy changes below zero ($\Delta G < 0$). Importantly, the comparison of the main thermodynamic parameters between SPR-1 and LPS showed that ΔG values of SPR-1 became more negative than that of the LPS (−6.17 kcal/mol vs. −7.82 kcal/mol), resulting in the K_D of the LPS (2.75 μM) small than the SPR-1 (18.8 μM). The K_D value of LPS determined in this experiment was generally consistent with those previously reported [72]. The above results suggested that the binding of LPS to MD2 was stronger than that of SPR-1, and also provided evidence for the direct interaction between SPR-1 and MD2. This novel finding indicated that a potential mechanism by which SPR-1 activated immunomodulatory effects was through direct interaction with MD2 to activate MD2/TLR4 signaling. Therefore, SPR-1 had the potential to be developed into a novel TLR4 agonist.

3.3.2. Molecular docking of SPR-1 and LPS with MD2

There is an essential role that TLR4 plays in pathogen recognition and innate immunity [71]. Most TLR4 activators currently in both clinical and preclinical studies are derivatives of its prototypic ligand LPS. The discovery of new TLR4 activators has the possibility for development as novel therapeutic immunomodulators and adjuvants. Co-receptors MD2 are essential for TLR4 signaling, binding to LPS and promoting TLR4 dimerization or oligomerization and activation of downstream signaling [71,73]. Therefore, we further predicted the possible binding sites of SPR-1 and LPS to MD2 to explore the possibility of SPR-1 as a TLR4 agonist. To this end, molecular docking was performed to predict the potential binding between SPR-1 and LPS with MD2 protein. Since MD2 was exceptionally flexible, and the clamshell-like motion of its β-cup folding allowed it to adapt to the size and shape of the bound ligand in the hydrophobic cavity. Hydrophobic and hydrogen were shown to be the most significant interactions of the binding mode. As shown in Figs. 7C—H, 17 hydrogen bonds were formed between SPR-1 and MD2, and 12 hydrogen bonding interactions were formed between LPS and MD2. Moreover, the aminoacidic active site residues for MD2 (Tyr102, Ser118, Ser120, Lys122, and Gly123) were reported in the literature, which was involved in the binding of LPS to the TLR4/MD2 complex [74]. As shown in Table S4, our result showed that SPR-1 might directly bind to MD2 (binding energy −5.569 kcal/mol), which was very similar to the binding energy between LPS and MD2 (binding energy −5.470 kcal/mol). Meanwhile, further analysis revealed that SPR-1 had a similar binding site to the MD2 binding site of LPS, and the same hydrogen bonding acceptors and donors (Glu92, Val93, Arg96, Tyr102, Ser120) exist, which resulted in the formation of hydrogen bonding interactions between SPR-1 and amino acid residues in this site pocket. Meanwhile, the affinity of SPR-1 with MD2 was further improved due to the hydrophobicity of the ring structure of SPR-1 being able to form certain hydrophobic interactions with the amino acids around the binding pocket of MD2. Overall, the molecular docking results showed that both SPR-1 and LPS could bind in the MD2 with multiple binding sites and form a relatively high-affinity stable complex. This suggested that SPR-1 has the potential to act as a new TLR4 agonist and may be developed into a novel therapeutic immunomodulator and adjuvant.

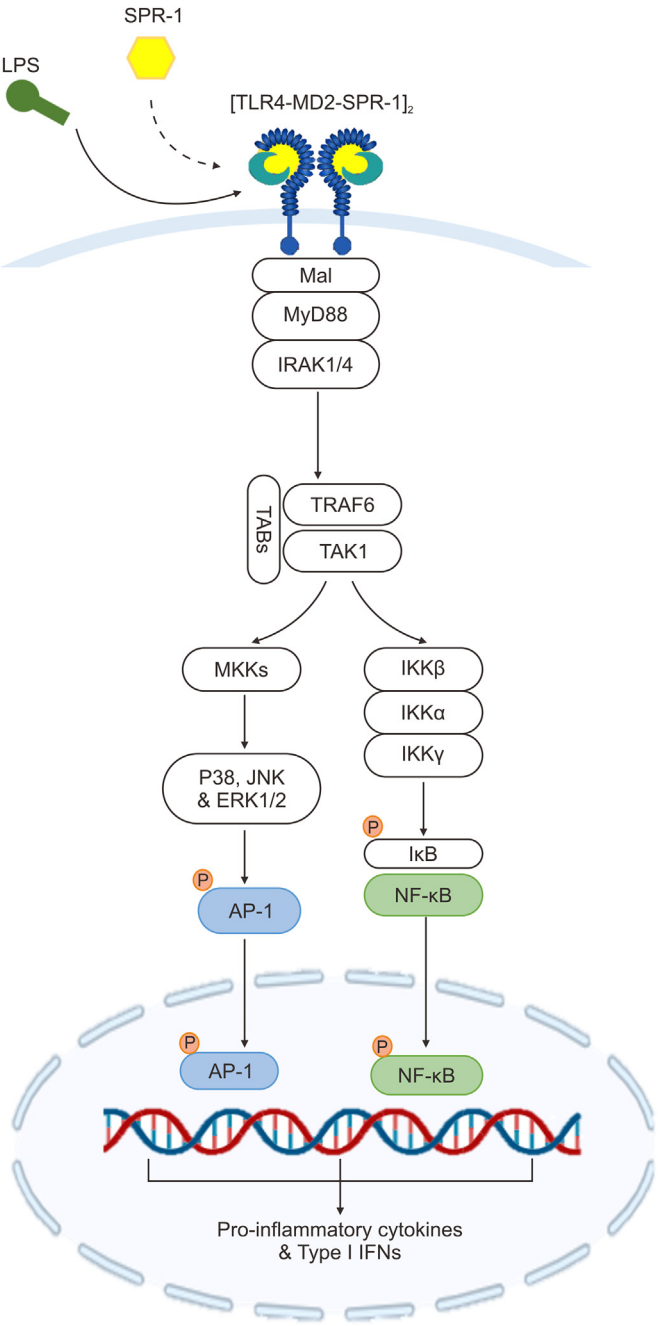

Fig. 8. Potential signaling pathways activated in macrophages treated with SPR-1. LPS: lipopolysaccharide; TLR4: Toll-like receptor 4; IRAK1/4: interleukin-1 receptor-associated kinase 1/4; TRAF6: TNF receptor associated factor 6; TAK1: transforming growth factor beta-activated kinase 1; MKKs: mitogen-activated protein kinase kinases; IKK: IκB kinase; JNK: c-Jun N-terminal kinase; ERK: extracellular regulated kinase; NF-κB: nuclear factor-kappa-B; AP-1: activating protein 1; IFNs: interferons.

4. Conclusion

In this study, a novel acidic polysaccharide SPR-1 with a Gal backbone (M_W of 3622 Da), which is mainly composed of Gal, Glc, and GalA, was purified from PRWB. The structural identification suggested that the backbone of SPR-1 might be consisted of [(4)-β-D-Gal*p*-(1]$_9$ → 4,6)-β-D-Gal*p*-(1 → 4)-α-D-GalA*p*-(1 → 4)-α-D-GalA*p*-(1 → 4)-α-D-Glc*p*-(1 → 4,6)-α-D-Glc*p*-(1 → 4)-α/β-D-Glc*p*, and the connection of the branch chains were R_1: β-D-Gal*p*-(1 → 3)-β-D-Gal*p*-(1→ and R_2: α-D-Glc*p*-(1 → 6)-α-D-Glc*p*-(1→.

Macrophages, an essential representative of immune function in the progress of cancer, constitute the first line of host immune defense, which serves antigen-presenting cells (APCs) and modulates the adaptive immune response [75,76]. The results revealed that SPR-1 polysaccharide could increase cytokine NO, IL-1β and TNF-α production by increasing the expression of iNOS, TNF-α, COX-2 and other genes in macrophages to stimulate the cellular production of the immune response. As a naturally produced drug, SPR-1 presented almost no cytotoxic effects even in a high concentration. Moreover, the above results suggested that iNOS and COX-2 might play a vital role in SPR-1-induced macrophage activation through the TLR4 and the NF-κB signaling pathways (Fig. 8). The ITC results illustrated that SPR-1 was able to directly bind to MD2 with a K_D of 18.8 μM. Multiple binding sites for SPR-1 and MD2 were indicated by molecular docking. It was suggested that SPR-1 has potential as a TLR4 agonist. Therefore, the elucidation of SPR-1 structural characteristics and immunomodulatory effects contributes to our understanding of its potential applications in various therapeutic interventions and further exploration of its biomedical potential.

In addition, the bioactivities of functional polysaccharides are primarily influenced by structural features, such as molecular weight, the type of glycosidic bonds, and the linkage method of main chain glycosidic bonds. Nevertheless, these are partially lacking in our current study. Further studies will be conducted to explore the complete structural feature-activity relationship and the mechanism of SPR-1 activation of immunomodulation *in vivo*.

CRediT authorship contribution statement

Hongna Su: Conceptualization, Methodology, Investigation, Data curation, Writing - Original draft preparation; **Lili He**: Resources, Investigation, Data curation; **Xina Yu**: Resources, Data curation; **Yue Wang**: Validation, Data curation; **Li Yang**: Validation, Data curation; **Pei Luo**: Resources, Writing - Reviewing and Editing; **Zhifeng Zhang**: Conceptualization, Supervision, Writing - Reviewing and Editing, Project administration.

Declaration of competing interest

The authors declare that there are no conflicts of interest.

Acknowledgments

This work was supported by Sichuan Provincial Regional Innovation Cooperation Project, China (Grant No.: 2023YFQ0084) and the Macau Science and Technology Development Fund (FDCT), China (Grant No.: 0043/2021/AGJ).

Appendix A. Supplementary data

Supplementary data to this article can be found online at https://doi.org/10.1016/j.jpha.2024.100974.

References

[1] L. Zhai, X. Wang, Syringaresinol-di-O-β-D-glucoside, a phenolic compound from *Polygonatum sibiricum*, exhibits an antidiabetic and antioxidative effect on a streptozotocin-induced mouse model of diabetes, Mol. Med. Rep. 18 (2018) 5511–5519.
[2] L. He, B. Yan, C. Yao, et al., Oligosaccharides from *Polygonatum* Cyrtonema *Hua*: Structural characterization and treatment of LPS-induced peritonitis in mice, Carbohydr. Polym. 255 (2021), 117392.
[3] X. Li, R. Ma, F. Zhang, et al., Evolutionary research trend of *Polygonatum* species: A comprehensive account of their transformation from traditional medicines to functional foods, Crit. Rev. Food Sci. Nutr. 63 (2023) 3803–3820.
[4] H. Gong, X. Gan, Y. Li, et al., Review on the genus *Polygonatum* polysaccharides: Extraction, purification, structural characteristics and bioactivities, Int. J. Biol. Macromol. 229 (2023) 909–930.
[5] R. Li, A. Tao, R. Yang, et al., Structural characterization, hypoglycemic effects and antidiabetic mechanism of a novel polysaccharides from *Polygonatum kingianum* Coll. et Hemsl, Biomed. Pharmacother. 131 (2020), 110687.
[6] J. Liu, T. Li, H. Chen, et al., Structural characterization and osteogenic activity *in vitro* of novel polysaccharides from the rhizome of *Polygonatum sibiricum*, Food Funct. 12 (2021) 6626–6636.
[7] H. Ren, Y. Deng, J. Zhang, et al., Research progress on processing history evolution, chemical components and pharmacological effects of Polygonati Rhizoma, Zhongguo Zhong Yao Za Zhi 45 (2020) 4163–4182.
[8] J. Zhang, Y. Wang, W. Yang, et al., Research progress in chemical constituents in plants of *Polygonatum* and their pharmacological effects, Zhongguo Zhong Yao Za Zhi 44 (2019) 1989–2008.
[9] J. Zhang, H. Chen, L. Luo, et al., Structures of fructan and galactan from *Polygonatum cyrtonema* and their utilization by probiotic bacteria, Carbohydr. Polym. 267 (2021), 118219.
[10] Z. Chen, L. Hu, Y. Liao, et al., Different processed products of curcumae *Radix* regulate pain-related substances in a rat model of qi stagnation and blood stasis, Front. Pharmacol. 11 (2020), 242.
[11] T. Sun, H. Zhang, Y. Li, et al., Physicochemical properties and immunological activities of polysaccharides from both crude and wine-processed *Polygonatum sibiricum*, Int. J. Biol. Macromol. 143 (2020) 255–264.
[12] J. Zhang, J. Wang, L. Yang, et al., Comprehensive quality evaluation of *Polygonatum cyrtonema* and its processed product: Chemical fingerprinting, determination and bioactivity, Molecules 28 (2023), 4341.
[13] X. Cheng, H. Ji, X. Cheng, et al., Characterization, classification, and authentication of *Polygonatum sibiricum* samples by volatile profiles and flavor properties, Molecules 27 (2021), 25.
[14] Y. Luan, Y. Jiang, R. Huang, et al., Polygonati rhizoma polysaccharide prolongs lifespan and healthspan in *Caenorhabditis elegans*, Molecules 28 (2023), 2235.
[15] Q. Li, J. Zeng, P. Gong, et al., Effect of steaming process on the structural characteristics and antioxidant activities of polysaccharides from *Polygonatum sibiricum* rhizomes, Glycoconj. J. 38 (2021) 561–572.
[16] X. Wang, G. Zhao, C. Ju, et al., Reduction of emodin-8-O-ß-D-glucoside content participates in processing-based detoxification of polygoni multiflori radix, Phytomed. Int. J. Phytother. Phytopharm. 114 (2023), 154750.
[17] Q. Qu, Z. Li, Q. Zhou, et al., Research progress on fermented traditional Chinese medicine and its theoretical exploration of "fermentation compatibility", Chin. Tradit. Herb. Drugs. 54 (2023) 2262–2273.
[18] P. Zhao, H. Zhou, C. Zhao, et al., Purification, characterization and immunomodulatory activity of fructans from *Polygonatum odoratum* and P. cyrtonema, Carbohydr. Polym. 214 (2019) 44–52.
[19] L. Xie, M. Shen, Y. Hong, et al., Chemical modifications of polysaccharides and their anti-tumor activities, Carbohydr. Polym. 229 (2020), 115436.
[20] W. Li, X. Hu, S. Wang, et al., Characterization and anti-tumor bioactivity of astragalus polysaccharides by immunomodulation, Int. J. Biol. Macromol. 145 (2020) 985–997.
[21] T. Guo, Y. Yang, M. Gao, et al., *Lepidium meyenii* Walpers polysaccharide and its cationic derivative re-educate tumor-associated macrophages for synergistic tumor immunotherapy, Carbohydr. Polym. 250 (2020), 116904.
[22] R. Zhang, X. Zhang, Y. Tang, et al., Composition, isolation, purification and biological activities of *Sargassum fusiforme* polysaccharides: A review, Carbohydr. Polym. 228 (2020), 115381.
[23] H. Tian, Z. Liu, Y. Pu, et al., Immunomodulatory effects exerted by *Poria cocos* polysaccharides via TLR4/TRAF6/NF-κB signaling *in vitro* and *in vivo*, Biomedecine Pharmacother 112 (2019), 108709.
[24] Y. Liu, Y. Ye, X. Hu, et al., Structural characterization and anti-inflammatory activity of a polysaccharide from the lignified okra, Carbohydr. Polym. 265 (2021), 118081.
[25] Y. Sun, J. Huo, S. Zhong, et al., Chemical structure and anti-inflammatory activity of a branched polysaccharide isolated from *Phellinus baumii*, Carbohydr. Polym. 268 (2021), 118214.
[26] S. Chen, X. Guan, T. Yong, et al., Structural characterization and hepatoprotective activity of an acidic polysaccharide from *Ganoderma lucidum*, Food Chem. X 13 (2022), 100204.
[27] S. Teng, Y. Zhang, X. Jin, et al., Structure and hepatoprotective activity of Usp10/NF-κB/Nrf2 pathway-related *Morchella esculenta* polysaccharide, Carbohydr. Polym. 303 (2023), 120453.
[28] Y. Ying, W. Hao, Immunomodulatory function and anti-tumor mechanism of natural polysaccharides: A review, Front. Immunol. 14 (2023), 1147641.

[29] N. Liu, Z. Dong, X. Zhu, et al., Characterization and protective effect of *Polygonatum sibiricum* polysaccharide against cyclophosphamide-induced immunosuppression in Balb/c mice, Int. J. Biol. Macromol. 107 (2018) 796–802.
[30] Z. Chen, J. Liu, X. Kong, et al., Characterization and immunological activities of polysaccharides from *Polygonatum sibiricum*, Biol. Pharm. Bull. 43 (2020) 959–967.
[31] L. Su, X. Li, Z. Guo, et al., Effects of different steaming times on the composition, structure and immune activity of *Polygonatum* Polysaccharide, J. Ethnopharmacol. 310 (2023), 116351.
[32] Y. Deng, J. Zhao, S. Li, Quantitative estimation of enzymatic released specific oligosaccharides from *Hericium erinaceus* polysaccharides using CE-LIF, J. Pharm. Anal. 13 (2023) 201–208.
[33] S. Zhang, X. Li, Inhibition of α-glucosidase by polysaccharides from the fruit hull of *Camellia oleifera* Abel, Carbohydr. Polym. 115 (2015) 38–43.
[34] Y. Wan, T. Hong, H. Shi, et al., Probiotic fermentation modifies the structures of pectic polysaccharides from carrot pulp, Carbohydr. Polym. 251 (2021), 117116.
[35] Y. Cui, Y. Chen, S. Wang, et al., Purification, structural characterization and antioxidant activities of two neutral polysaccharides from persimmon peel, Int. J. Biol. Macromol. 225 (2023) 241–254.
[36] X. Li, Q. Chen, G. Liu, et al., Chemical elucidation of an Arabinogalactan from rhizome of *Polygonatum sibiricum* with antioxidant activities, Int. J. Biol. Macromol. 190 (2021) 730–738.
[37] B. Dai, D. Wei, N. Zheng, et al., *Coccomyxa* gloeobotrydiformis polysaccharide inhibits lipopolysaccharide-induced inflammation in RAW 264.7 macrophages, Cell. Physiol. Biochem. 51 (2018) 2523–2535.
[38] S. Zhang, X. Li, B. Ai, et al., Binding of β-lactoglobulin to three phenolics improves the stability of phenolics studied by multispectral analysis and molecular modeling, Food Chem. X 15 (2022), 100369.
[39] R. Khanam, I.I. Hejazi, S. Shahabuddin, et al., Pharmacokinetic evaluation, molecular docking and *in vitro* biological evaluation of 1, 3, 4-oxadiazole derivatives as potent antioxidants and STAT3 inhibitors, J. Pharm. Anal. 9 (2019) 133–141.
[40] T. Li, R. Guo, Q. Zong, et al., Application of molecular docking in elaborating molecular mechanisms and interactions of supramolecular cyclodextrin, Carbohydr. Polym. 276 (2022), 118644.
[41] S. Qin, X. Huang, S. Qu, Baicalin induces a potent innate immune response to inhibit respiratory syncytial virus replication *via* regulating viral non-structural 1 and matrix RNA, Front. Immunol. 13 (2022), 907047.
[42] Z. Mai, W. Wei, H. Yu, et al., Molecular recognition of the interaction between ApoE and the TREM2 protein, Transl. Neurosci. 13 (2022) 93–103.
[43] Y. Liu, T. Tang, S. Duan, et al., The purification, structural characterization and antidiabetic activity of a polysaccharide from *Anoectochilus roxburghii*, Food Funct. 11 (2020) 3730–3740.
[44] Y. Tian, Y. Zhao, H. Zeng, et al., Structural characterization of a novel neutral polysaccharide from *Lentinus giganteus* and its antitumor activity through inducing apoptosis, Carbohydr. Polym. 154 (2016) 231–240.
[45] J. Jin, J. Lao, R. Zhou, et al., Simultaneous identification and dynamic analysis of saccharides during steam processing of rhizomes of *Polygonatum cyrtonema* by HPLC-QTOF-MS/MS, Molecules 23 (2018), 2855.
[46] H. Zhan, F. Yao, B. Yi, et al., Exploring the differences of Polygonati Rhizoma before and after stewing based on carbohydrate components, Chinese Traditional and Herbal Drugs 53 (2022) 2687–2696.
[47] Y. Wang, N. Liu, X. Xue, et al., Purification, structural characterization and *in vivo* immunoregulatory activity of a novel polysaccharide from *Polygonatum sibiricum*, Int. J. Biol. Macromol. 160 (2020) 688–694.
[48] H. Jiang, Y. Xu, C. Sun, et al., Physicochemical properties and antidiabetic effects of a polysaccharide obtained from *Polygonatum odoratum*, Int. J. Food Sci. Technol. 53 (2018) 2810–2822.
[49] L. Huang, J. Zhao, Y. Wei, et al., Structural characterization and mechanisms of macrophage immunomodulatory activity of a pectic polysaccharide from *Cucurbita moschata* Duch, Carbohydr. Polym. 269 (2021), 118288.
[50] A. Naeem, C. Yu, W. Zhu, et al., Study of hydroxypropyl β-cyclodextrin and puerarin inclusion complexes encapsulated in sodium alginate-grafted 2-acrylamido-2-methyl-1-propane sulfonic acid hydrogels for oral controlled drug delivery, Gels 9 (2023), 246.
[51] X. Liu, Z. Zhu, Y. Tang, et al., Structural properties of polysaccharides from cultivated fruit bodies and mycelium of *Cordyceps militaris*, Carbohydr. Polym. 142 (2016) 63–72.
[52] Y. Peng, L. Zhao, K. Hu, et al., Anti-fatigue effects of *Lycium barbarum* polysaccharide and effervescent tablets by regulating oxidative stress and energy metabolism in rats, Int. J. Mol. Sci. 23 (2022), 10920.
[53] H. Jiang, H. Zhu, G. Huo, et al., *Oudemansiella raphanipies* polysaccharides improve lipid metabolism disorders in murine high-fat diet-induced non-alcoholic fatty liver disease, Nutrients 14 (2022), 4092.
[54] Z. Zhu, X. Song, Y. Jiang, et al., Chemical structure and antioxidant activity of a neutral polysaccharide from Asteris *Radix* et Rhizoma, Carbohydr. Polym. 286 (2022), 119309.
[55] F. Li, Y. Wei, L. Liang, et al., A novel low-molecular-mass pumpkin polysaccharide: Structural characterization, antioxidant activity, and hypoglycemic potential, Carbohydr. Polym. 251 (2021), 117090.
[56] Y. Ru, X. Chen, J. Wang, et al., Structural characterization, hypoglycemic effects and mechanism of a novel polysaccharide from *Tetrastigma hemsleyanum* Diels et Gilg, Int. J. Biol. Macromol. 123 (2019) 775–783.
[57] B. Li, F. Lu, H. Nan, et al., Isolation and structural characterisation of okara polysaccharides, Molecules 17 (2012) 753–761.
[58] E.L. Nazarenko, R.J. Crawford, E.P. Ivanova, The structural diversity of carbohydrate antigens of selected gram-negative marine bacteria, Mar. Drugs 9 (2011) 1914–1954.
[59] H. Li, T. Gao, Z. Zhang, et al., A novel *Stauntonia leucantha* fruits Arabinogalactan: And structural characterization, Carbohydr. Polym. 303 (2023), 120481.
[60] X. Ma, L. Dong, Y. He, et al., Effects of ultrasound-assisted H_2O_2 on the solubilization and antioxidant activity of yeast β-glucan, Ultrason. Sonochem. 90 (2022), 106210.
[61] Y. Yang, X. Yin, D. Zhang, et al., Structural characteristics, antioxidant, and immunostimulatory activities of an acidic polysaccharide from raspberry pulp, Molecules 27 (2022), 4385.
[62] Z. Yin, X. Liu, J. Wang, et al., Structural characterization and anticoagulant activity of a 3-*O*-methylated heteroglycan from fruiting bodies of *Pleurotus placentodes*, Front. Chem. 10 (2022), 825127.
[63] X. Guan, Q. Wang, B. Lin, et al., Structural characterization of a soluble polysaccharide SSPS1 from soy whey and its immunoregulatory activity in macrophages, Int. J. Biol. Macromol. 217 (2022) 131–141.
[64] C. Limban, A.V. Missir, K.M. Fahelelbom, et al., Novel N-phenylcarbamothioylbenzamides with anti-inflammatory activity and prostaglandin E2 inhibitory properties, Drug Des. Devel. Ther. 7 (2013) 883–892.
[65] A. Dénou, A. Togola, K.T. Inngjerdingen, et al., Isolation, characterisation and complement fixation activity of acidic polysaccharides from *Argemone mexicana* used as antimalarials in Mali, Pharm. Biol. 60 (2022) 1278–1285.
[66] X. Qi, Y. Yu, X. Wang, et al., Structural characterization and anti-oxidation activity evaluation of pectin from *Lonicera japonica* Thunb, Front. Nutr. 9 (2022), 998462.
[67] X. Wei, J. Yao, F. Wang, et al., Extraction, isolation, structural characterization, and antioxidant activity of polysaccharides from elderberry fruit, Front. Nutr. 9 (2022), 947706.
[68] Y. Xie, L. Wang, H. Sun, et al., Polysaccharide from alfalfa activates RAW 264.7 macrophages through MAPK and NF-κB signaling pathways, Int. J. Biol. Macromol. 126 (2019) 960–968.
[69] S.S. Ferreira, C.P. Passos, P. Madureira, et al., Structure-function relationships of immunostimulatory polysaccharides: A review, Carbohydr. Polym. 132 (2015) 378–396.
[70] Y. Xie, L. Wang, H. Sun, et al., A polysaccharide extracted from alfalfa activates splenic B cells by TLR4 and acts primarily *via* the MAPK/p38 pathway, Food Funct. 11 (2020) 9035–9047.
[71] A. Michaeli, S. Mezan, A. Kühbacher, et al., Computationally designed bispecific MD2/CD14 binding peptides show TLR4 agonist activity, J. Immunol. 201 (2018) 3383–3391.
[72] H.J. Shin, H. Lee, J.D. Park, et al., Kinetics of binding of LPS to recombinant CD14, TLR4, and MD-2 proteins, Mol. Cells 24 (2007) 119–124.
[73] Y. Wang, Y. Qian, Q. Fang, et al., Saturated palmitic acid induces myocardial inflammatory injuries through direct binding to TLR4 accessory protein MD2, Nat. Commun. 8 (2017), 13997.
[74] Q.U. Ain, M. Batool, S. Choi, TLR4-targeting therapeutics: Structural basis and computer-aided drug discovery approaches, Molecules 25 (2020), 627.
[75] Y. Liu, L. Li, Y. Li, et al., Research progress on tumor-associated macrophages and inflammation in cervical cancer, BioMed Res. Int. 2020 (2020), 6842963.
[76] W. Wei, L. Feng, W. Bao, et al., Structure characterization and immunomodulating effects of polysaccharides isolated from *Dendrobium officinale*, J. Agric. Food Chem. 64 (2016) 881–889.